Applied Energy, Vol. 205, 1 November 2017, pp. 1189-1201
DOI:10.1016/j.apenergy.2017.08.090

High-efficiency negative-carbon emission power generation from integrated solid-oxide fuel cell and calciner

Dawid P. Hanak[1], Barrie G. Jenkins[2], Tim J. R. Kruger[3] and Vasilije Manovic[1]*

[1]Combustion and CCS Centre, Cranfield University, Bedford, Bedfordshire, MK43 0AL, UK

[2]Consulting Engineers, High Wycombe, Buckinghamshire, HP11 2TH, UK

[3]Origen Power Ltd, Aldridge, Walsall, West Midlands, WS9 8LZ, UK

Applied Energy, 205, 2017, 1189–1201

Corresponding author: *Dawid P. Hanak, d.p.hanak@cranfield.ac.uk

Abstract

Direct air capture of CO_2 has the potential to help meet the ambitious environmental targets established by the Paris Agreement. This study assessed the techno-economic feasibility of a process for simultaneous power generation and CO_2 removal from the air using solid sorbents. The process uses a solid-oxide fuel cell to convert the chemical energy of fuel to electricity and high-grade heat, the latter of which can be utilised to calcine a carbonate material that, in turn, can remove CO_2 from the air. The proposed process was shown to operate with a net thermal efficiency of 43.7–47.7%$_{LHV}$ and to have the potential to remove 463.5–882.3 $gCO_2/kW_{el}h$, depending on the fresh material used in the calciner. Importantly, the estimated capital cost of the proposed process (1397.9–1740.5 £/$kW_{el,gross}$) was found to be lower than that for other low-carbon emission power generation systems using fossil fuels. The proposed process was also shown to achieve a levelised cost of electricity of 50 £/$MW_{el}h$, which is competitive with other low-carbon power generation technologies, for a carbon tax varying between 39.2 and 74.9 £/tCO_2. Such figure associated with the levelised cost of CO_2 capture from air is lower than for other direct air concepts.

Key Words: Direct air capture**,** solid-oxide fuel cell, power generation, process modelling and simulation, feasibility study, techno-economic analysis

1 INTRODUCTION

The Paris Agreement, reached at the 21st Conference of the Parties, has suggested that to significantly reduce the risks and impacts of climate change, the global mean temperature increase needs to be held well below 2°C and efforts to limit it to 1.5°C above pre-industrial levels need to be pursued [1]. To achieve this ambitious goal, the recent scenarios imply that negative emissions technologies, such as bioenergy with carbon capture and storage, direct air capture (DAC), and enhanced weathering of minerals, need to be widely deployed, although they are only in the early development phase [2–6].

The concept of DAC, which was initially proposed by Lackner et al. [7], has some distinctive features that make it viable for wide deployment. Primarily, as DAC does not need to be located at the emission source, it has potential to address emissions from point and distributed sources, including emissions from agriculture, buildings and transportation sectors that account roughly for half of the annual anthropogenic CO_2 emissions [8], [9]. Furthermore, the gas to be treated in DAC – ambient air – contains low amounts of SO_x and NO_x, which implies lower degradation of the sorbent compared to CO_2 capture from combustion flue gases [8,10,11]. The main disadvantage of DAC is, however, an extremely low concentration of CO_2 in the ambient air of about 400 ppm, which is about 350 times lower than the CO_2 concentration in the flue gas from the combustion of coal [8]. For this reason, the cost of removing CO_2 from ambient air was estimated to range between 400 £/tCO_2 [12] and 800 £/tCO_2 [13], which is an order of magnitude higher than figures reported for CO_2 capture from combustion processes [14]. Nevertheless, DAC is regarded as potentially important in alleviating the effects of anthropogenic CO_2 emissions in the long term, should the direct removal of CO_2 from air be required to stabilise the CO_2

concentration at a desired level [13,15,16]. Importantly, DAC is not currently an economically feasible technology and is expected to be deployed only after 2050, by which time the centralised CO_2 emitters will have been completely decarbonised [17,18].

A number of DAC concepts employing natural inorganic materials, including regenerative processes using strong bases such as NaOH in Na/Ca, KOH in K/Ca, and $Ca(OH)_2$ in $CaO/Ca(OH)_2/CaCO_3$ cycles [11,19,20], have been evaluated and found to be effective in scrubbing CO_2 from the ambient air. However, these processes are energy intensive and require very high regeneration temperatures [11]. This is because the sorbent regeneration is conducted via calcination of the $CaCO_3$ that takes place at temperatures above 700°C, usually 800–950°C depending on the CO_2 partial pressure in the gas stream leaving the calciner [21]. To maintain a high purity of the concentrated CO_2 stream, the calcination process is usually driven by the direct oxy-combustion of fuel in the calciner [8,11]. This introduces the main source of the parasitic load in the process, as O_2 production is usually conducted in a cryogenic air separation unit that is characterised with a specific power requirement of 184–230 $kW_{el}h/tO_2$ [22–24]. The main alternative options to drive the calcination process include chemical looping [25–28], which uses oxygen carriers to transfer oxygen from air to the fuel, and indirect heat transfer from a combustor via solid heat carriers [29,30], heat transfer wall [30,31] or heat pipes [32,33].

This study proposes to utilise the high-grade heat from a solid-oxide fuel cell (SOFC) to drive the calcination process in a once-through DAC concept. In contrast to the other high-temperature DAC concepts, the proposed process will generate electricity at a high efficiency, in addition to capturing CO_2 from the ambient air and producing a concentrated CO_2 stream. As a result, the proposed process is expected to be more economically viable compared to the DAC concepts reported in the literature. Importantly, such process will be incorporated in the Balanced Energy Network (BEN) project that aims to demonstrate a heating, cooling and electricity network that minimises the cost and CO_2 emissions by balancing the delivery of these energy vectors. Therefore, to assess the process feasibility, a techno-economic analysis and parametric studies on the key design parameters are performed in this study. Furthermore, the effect of the sorbent composition on the techno-economic performance is assessed for a range of natural materials.

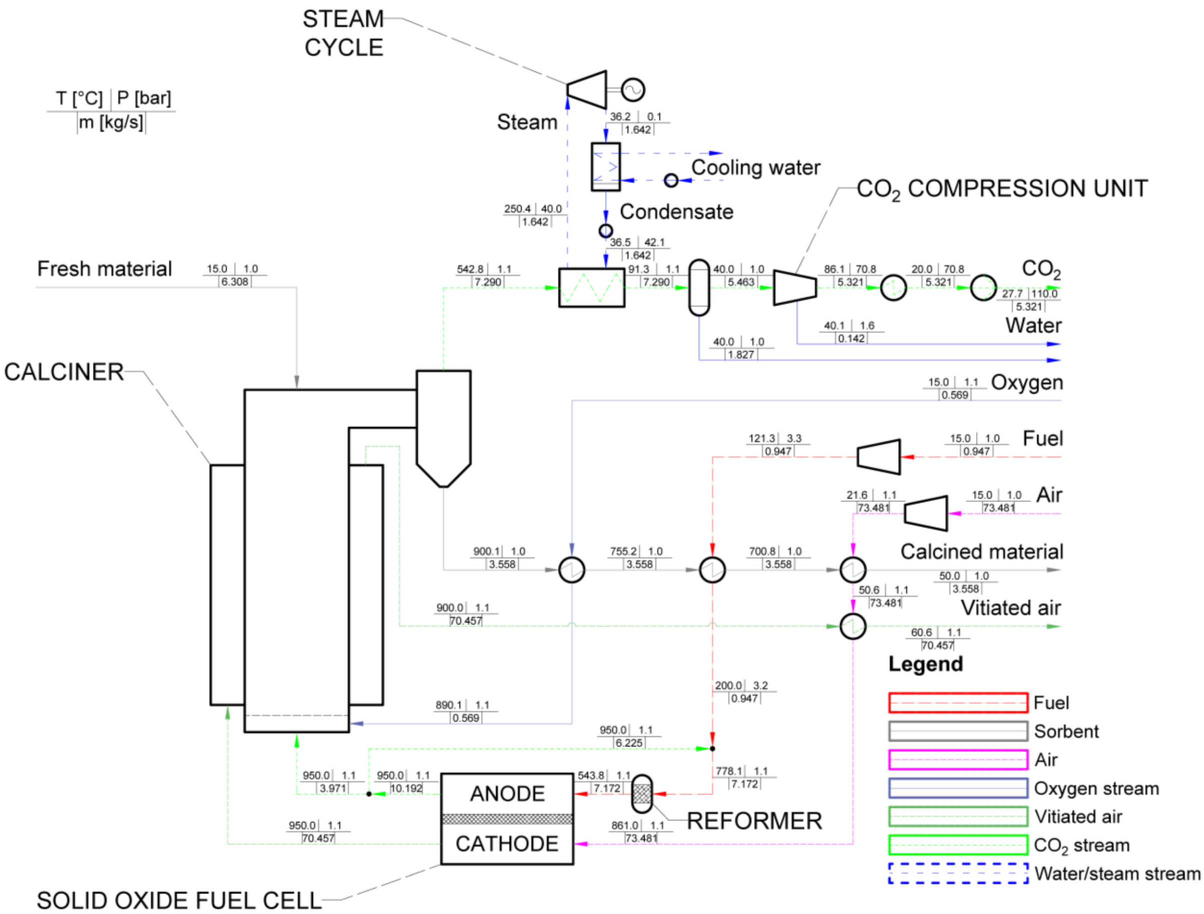

Figure 1: Process flow diagram of the process for simultaneous power generation and direct CO_2 removal from the air*

* Stream data in this figure refers to the system in which limestone was fed to the calciner as a fresh material. The stream data and overall energy balances for all systems are provided in Supplementary Information.

2 MODEL DEVELOPMENT

2.1 Process description

The process for simultaneous power generation and CO_2 removal from the air (Figure 1) comprises four distinct sub-systems: fresh material calciner, heat recovery system including a simple steam cycle, CO_2 compression unit (CCU), and SOFC. The main principle behind the proposed process is to use the SOFC to generate electricity with a high efficiency and produce heat for calcination of the fresh material. The calcined material can then be used for direct air capture, which is expected to take place in the open environment, enabling negative CO_2 emissions.

The core of the process is the flash calciner, where the fresh material is decomposed upon heating. The temperature at which the calcination takes place depends on the type of fresh material (Table 1) fed to the calciner. It varies between 550°C for magnesite and dolomite (partial calcination), through 850°C for dolomite (complete calcination), and to 900°C for limestone. Such operating temperatures have been selected based on the equilibrium curves for calcite and magnesite (Figure 2) [34,35]. These curves establish the operating temperature envelope for the calciner. Importantly, similar operating temperatures have been widely used in testing the physical and chemical properties, and resulted in nearly complete calcination of the materials considered in this study [36–39].

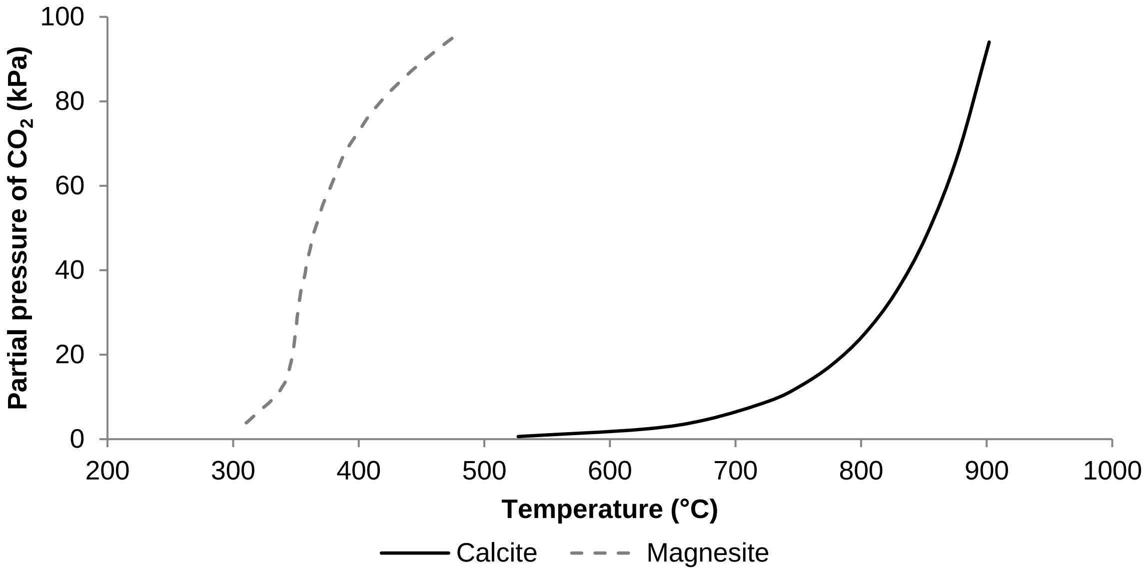

Figure 2: Variation of equilibrium CO_2 partial pressure of calcite and magnesite with temperature [34,35]

The amount of fresh material fed to the calciner is determined by the amount of high-grade heat available in the gas streams leaving the 25 $MW_{el,DC}$ SOFC, which uses natural gas as a fuel. This scale of the SOFC is comparable to existing combined heat and power plants, the scale of which ranges between 1 and 60 $MW_{el,AC}$ [40–43]. Importantly, in addition to producing electricity with a high net thermal efficiency (~49.8%$_{LHV}$), the SOFC generates vitiated air and CO_2/H_2O streams at a high temperature (950°C). As opposed to the power systems reported in the literature, in which the SOFC is linked with another power cycle, achieving net thermal efficiencies of up to 70% [44,45], the high-grade heat carried by these process streams is utilised to drive the calcination process. The main benefit of the proposed process is its potential to remove large amounts of CO_2 directly from air, which is not achievable by the SOFC-based power generation systems. Importantly, the CO_2/H_2O stream leaving the anode comprises only a small amount of trace gases from the fuel and, therefore, can be fed without any pre-treatment to the calciner for direct heat transfer with the sorbent. As the fuel is not completely utilised in the SOFC [46,47], pure O_2, which is produced in the air separation unit (ASU), is fed to the calciner to complete the fuel combustion. To keep the purity of the CO_2 stream at a level suitable for geological sequestration (>95%$_{vol}$ CO_2 [48]), the vitiated air leaving the cathode is not fed directly into the calciner. Instead, it indirectly provides heat to the calciner via a heat transfer jacket surrounding the reactor. Importantly, the streams leaving the calciner carry a significant amount of high-grade heat that can be utilised within the system.

As shown in Figure 1, the calcined material is collected from the reactor at the calcination temperature and is cooled against the O_2, fuel and air streams. It is then distributed in the open environment, as opposed to other approaches in which the carbonation takes place in the reactor, for CO_2 capture over an elongated period of time. The air stream is further heated to above 850°C against the vitiated air, prior to being fed to the SOFC. The heat carried by the CO_2/H_2O stream is partially utilised to preheat the fresh material fed to the calciner. To increase heat utilisation in the system, the residual heat is then utilised to raise saturated steam at 5–40 bar, depending on the CO_2/H_2O stream temperature, to generate an additional amount of electricity in the steam cycle, or to drive CO_2 compressors. Alternatively, the residual heat can be utilised in a district heating network, which is out of this study's scope. After dehydration, the concentrated CO_2 stream is compressed to 110 bar.

Table 1: Initial design conditions and thermodynamic model assumptions

Parameter		Value
Calciner	Gibbs reactor. Gibbs free energy minimisation model.	
	Temperature (°C)	550–900
	Pressure drop (mbar)	150
	Excess O_2 (%)	2
	Air separation unit specific power requirement ($kW_{el}h/tO_2$)	200
	Heat loss (%)	4
Solid-oxide fuel cell	Gibbs reactors for pre-reformer and anode. Component splitter for cathode. Linked with electrochemical calculator in MS Excel. Natural gas composition adapted from the revised NETL report [49].	
	Temperature (°C)	950
	Pressure (bar)	1.08
	Fuel utilisation (%)	85
	Reference conditions: Fuel composition (67%$_{vol}$ H_2, 22%$_{vol}$ CO, 11%$_{vol}$ H_2O), fuel utilisation (U_f=85%), air utilisation (U_a=25%), operating temperature (T=1000°C), Operating pressure (P=1 bar), H_2 to H_2O partial pressure ratio ($p_{H2,ref}/p_{H2O,ref}$=0.15), O_2 partial pressure at cathode ($p_{O2,ref}$=0.164)	
Saturated steam cycle	Design live steam pressure (bar)	40*
	Feedwater pressure (bar)	42*
	Terminal temperature difference in heat recovery steam generator (°C)	10
	Condenser operating pressure (bar)	0.06
	Isentropic efficiency of the steam turbine (%)	85
	Isentropic efficiency of boiler feedwater pump (%)	80
	Isentropic efficiency of cooling water pump (%)	85
	Mechanical efficiency of steam turbines (%)	99.6
	Mechanical efficiency of pumps (%)	99.6
	Generator efficiency (%)	98
Heat exchanger network	Minimum approach temperature in the O_2 preheater (°C)	10
	Fuel outlet temperature from the fuel preheater (°C)	200
	Calcined material outlet temperature from first air preheater (APX1) (°C)	50
	Minimum approach temperature in the second air preheater (APX2) (°C)	10
CO_2 compression unit	Intercooling temperature (°C)	40
	CO_2 delivery pressure (bar)	110
	Polytropic efficiency of CO_2 compressors (%)	77–80
	Isentropic efficiency of CO_2 pump (%)	85
	Mechanical efficiency of compressors and pump (%)	99.6
Fresh material	Limestone (95%$_{wt}$ $CaCO_3$, 3.5%$_{wt}$ $MgCO_3$, 0.6%$_{wt}$ SiO_2, 0.4%$_{wt}$ Fe_2O_3, 0.5%$_{wt}$ Al_2O_3)	
	Dolomite (57.5%$_{wt}$ $CaCO_3$, 42.44%$_{wt}$ $MgCO_3$, 0.01%$_{wt}$ SiO_2, 0.02%$_{wt}$ Fe_2O_3, 0.03%$_{wt}$ Al_2O_3)	
	Magnesite (4.49%$_{wt}$ $CaCO_3$, 91.99%$_{wt}$ $MgCO_3$, 2.88%$_{wt}$, SiO_2, 0.42%$_{wt}$ Fe_2O_3, 0.22%$_{wt}$ Al_2O_3)	
Fuel	Natural gas (93.1%$_{vol}$ CH_4, 3.2%$_{vol}$ C_2H_6, 0.7%$_{vol}$ C_3H_8, 0.4%$_{vol}$ C_4H_{10}, 1.0%$_{vol}$ CO_2, 1.6%$_{vol}$ N_2)	

*In the case of partial calcination of dolomite, the saturated steam and feedwater pressures are 5 and 5.3 bar, respectively.

2.2 Thermodynamic model description

The steady state model for the proposed process was developed in Aspen Plus® and comprises four main sub-systems: fresh material calciner, heat recovery system including a simple steam cycle, CO_2 compression unit, and SOFC. The Peng-Robinson-Boston-Mathias (PR-BM) equation of state was used to represent the solid and gas streams, while STEAMNBS steam table was used for water/steam streams in the saturated steam cycle.

2.2.1 Flash calciner

The flash calciner is modelled as two *Gibbs* reactors, one to represent the calcination process and another to represent the fresh material preheating against the CO_2/H_2O stream as well as the heat loss of 4% of the enthalpy entering the preheater. The heat required to sustain the calcination process is provided by the sensible heat of the CO_2/H_2O stream leaving the anode (direct heat transfer) and the vitiated air stream leaving the cathode (indirect heat transfer). The latter is modelled as a *Heater* linked with the first *Gibbs* reactor by the heat stream. Importantly, as indicated above, the amount of fresh material fed to the calciner is determined by the design specification to ensure that the calciner is in the heat balance. Moreover, the amount of O_2 required to ensure complete fuel utilisation is estimated by assuming 2% excess O_2. Although the ASU is not modelled in detail in this study, its contribution to the parasitic load is quantified using the specific power requirement of 200 $kW_{el}h/tO_2$.

2.2.2 Heat recovery system

The high-grade sensible heat of the CO_2/H_2O, vitiated air and calcined material streams is used in the heat recovery system comprising a heat exchanger network, which aims to ensure a high level of process heat utilisation within the system, and the simple steam cycle for residual heat utilisation. The heat exchanger network is designed as a set of four *HeatX* unit operations to preheat the air, O_2, and fuel streams, with the design specifications listed in Table 1. It is assumed that the overall heat transfer coefficient in the gas-solid and gas-gas heat exchangers is 100 and 50 W/m^2K, respectively.

The heat exchange sections in the saturated steam cycle model consist of the economiser and the evaporator modelled as *HeatX* unit operations that raise the saturated steam at 40 bar from the feedwater at 42 bar using the residual heat from the CO_2/H_2O stream. Importantly, in the case of partial calcination of dolomite at 550°C, the saturated steam and feedwater pressures are 5 and 5.3 bar, respectively. The amount of saturated steam is determined to ensure 10°C temperature approach in the heat recovery steam generator. The steam turbine (*Compr*) is characterised by an isentropic efficiency of 85% and a generator efficiency of 98% is also assumed. The wet steam discharged from the steam turbine is condensed in the condenser (*HeatX*) at 0.06 bar. It is assumed that the temperature increase of the cooling water is 10°C in the condenser. The condensate is pumped to 42 bar in the feedwater pump (*Pump*) characterised by an isentropic efficiency of 80%. The CO_2/H_2O stream leaving the steam generator is then dehumidified on cooling to 40°C in the water knock-out tank that is modelled as a *Flash2* tank.

2.2.3 CO_2 compression unit

It is established that the CO_2 stream pressure at ambient temperature for pipeline transport is 110 bar [50]. To minimise the power requirement of the CCU, it is assumed that the concentrated CO_2 stream produced in the calciner is first compressed to 80 bar, which is just over the critical pressure, due to the impurities content, cooled down to 25°C and then pumped to 110 bar prior to transport. The CCU is modelled as a set of nine compression stages, so that the pressure ratio and the polytropic head do not exceed 3 and 3050 m, respectively, to allow for equipment limitations [51]. Each compression stage consists of a centrifugal compressor, stage intercoolers and scrubbers. The CO_2 compression is modelled using the polytropic compression model with constant stage polytropic efficiency of 78–80% [52,53] and the pump characterised with an isentropic efficiency of 80%.

2.2.4 Solid-oxide fuel cell

The SOFC is modelled based on the zero-dimensional natural gas-fed tubular SOFC model developed in Aspen Plus® by Zhang et al. [47]. As illustrated in Figure 1, the fuel pressure is increased in the fuel compressor (*Compr*) to ensure the ejector fresh fuel pressure ratio (P_{fuel}/P_{SOFC}) of 3. The ejector (*Mixer*) mixes the fresh fuel with the recycled anode gas, the amount of which is determined by a specified ratio of steam and carbon (*S/C*) required by the reformer. Under initial design conditions, *S/C* is controlled by the design specification to be 2.5. The adiabatic pre-reformer is required to prevent carbon formation and large temperature gradients at the anode [54]. It is assumed that the steam reforming and water-gas shift reactions, which occur in this reactor, reach thermodynamic equilibrium. Therefore, the *Gibbs* reactor is used to model the adiabatic pre-reformer along with the design specification that estimates the reformer operating temperature at which its net heat duty is zero.

At high temperatures of around 1000°C, which are typical operating temperatures of SOFCs, the reforming of CH_4 to H_2 as well as water-gas shift of CO and H_2O to H_2 are more favoured than the direct oxidation of CH_4 and CO in the pre-reformed fuel. It is, therefore, expected that these reactions will take place along with the electrochemical reaction of H_2 and O_2 in the SOFC [55]. These reactions are assumed to reach thermodynamic equilibrium and are modelled using the *Gibbs* reactor operating at 950°C (T_{SOFC}), in order to ensure efficient heat transfer between the streams leaving the SOFC and the material in the calciner. The cathode, which separates O_2 from the preheated air for the electrochemical reaction, is modelled as a component splitter (*Sep*). The vitiated air is heated to the anode operating temperature in the *Heater* that is linked with the *Gibbs* reactor representing the anode by the heat stream. The amount of O_2 consumed in the anode ($\dot{n}_{O2,eq}$) is estimated using Eq. (1) based on the equivalent H_2 molar flow rate ($\dot{n}_{H2,eq}$), which is defined in Eq. (2) as the equivalent amount of H_2 in the fresh fuel, and the assumed fuel utilisation factor (U_f).

$$\dot{n}_{O_2,eq} = 0.5U_f\dot{n}_{H_2,eq} \tag{1}$$

$$\dot{n}_{H_2,eq} = \dot{n}_{H_2,in} + \dot{n}_{CO,in} + 4\dot{n}_{CH_4,in} + 7\dot{n}_{C_2H_6,in} + \ldots \tag{2}$$

The amount of air fed to the cathode is determined using the design specification that varies the air utilisation (U_a) in the cathode to arrive at the heat loss of 2% in the SOFC. As mentioned above, the amount of fuel that has not been utilised in the SOFC is combusted in pure O_2 in the calciner to ensure complete fuel utilisation and high purity of the concentrated CO_2 stream.

To evaluate the thermodynamic performance of the SOFC, its current and voltage are first determined. The SOFC current (I_{SOFC}) is estimated using Eq. (3) based on the equivalent H_2 molar flow rate, fuel utilisation, Faraday constant (F), and number of electrons produced per mole of H_2 reacted (e). Moreover, the active area of the SOFC (AC_{SOFC}) is estimated from the SOFC current and assumed current density (I_C) of 250 mA/cm^2.

$$I_{SOFC} = \frac{en_{H_2,eq}FU_f}{3.6} \tag{3}$$

Estimation of the SOFC voltage utilises a performance curve that represents the experimental data at standard operating conditions for the reference system. In this study, the reference voltage (V_{ref}) is estimated for a desired current density using experimental data published in Fuel Cell Handbook [55] for the reference operating conditions listed in Table 1. The actual SOFC voltage (V_{SOFC}) is then calculated using Eq. (4) that employs semi-empirical correlations presented in Eq. (5) to Eq. (8) to correct the reference voltage due to variation in the actual pressure (ΔV_p), temperature and current density (ΔV_T), fuel composition (ΔV_{anode}), and oxidant composition ($\Delta V_{cathode}$) [47,55].

$$V_{SOFC} = V_{ref} + \Delta V_p + \Delta V_T + \Delta V_{anode} + \Delta V_{cathode} \tag{4}$$

$$\Delta V_p = 76 log \frac{P_{SOFC}}{P_{ref}} \tag{5}$$

$$\Delta V_T = 0.008(T_{SOFC} - T_{ref}) I_c \tag{6}$$

$$\Delta V_{anode} = 172 log \frac{P_{H_2}/P_{H_2O}}{P_{H_2,ref}/P_{H_2O,ref}} \tag{7}$$

$$\Delta V_{cathode} = 92 log \frac{P_{O_2}}{P_{O_2,ref}} \tag{8}$$

$$\dot{W}_{SOFC,AC} = \eta_{DC/AC} I_{SOFC} V_{SOFC} = \eta_{DC/AC} \dot{W}_{SOFC,DC} \tag{9}$$

The SOFC model utilises a design specification that adjusts the fuel flow rate to arrive at the rated power output of 25 $MW_{el,DC}$ ($\dot{W}_{SOFC,DC}$). The actual power output of the SOFC ($\dot{W}_{SOFC,AC}$) is calculated using Eq. (9), considering SOFC voltage, current, and DC-to-AC inverter efficiency ($\eta_{DC/AC}$). The prediction generated by the SOFC model developed in this study was found to reflect the data reported in the literature (Appendix A).

3 FEASIBILITY ASSESSMENT

3.1 Key techno-economic performance indicators

The thermodynamic performance of the proposed process for simultaneous power generation and CO_2 removal from the air is characterised using the key performance indicators that are commonly used to assess the performance of conventional power generation systems. These are primarily the net power output ($\dot{W}_{net}$), which accounts for the power output from the SOFC and the steam cycle less any parasitic load, and net thermal efficiency (η_{th}). The latter is defined in Eq. (10) as the ratio of the net power output and the chemical energy input to the system, which is calculated as the product of the fuel consumption rate ($\dot{m}_{fuel}$) and its lower heating value (*LHV*). Environmental performance is quantified in terms of the specific negative CO_2 emissions (e_{CO2}) defined in Eq. (11) as the ratio of the potential CO_2 removal rate from the atmosphere ($\dot{m}_{CO2}$) and the net power output.

$$\eta_{th} = \frac{\dot{W}_{net}}{\dot{m}_{fuel} LHV} \tag{10}$$

$$e_{CO_2} = \frac{\dot{m}_{CO_2}}{\dot{W}_{net}} \tag{11}$$

The economic performance of the proposed process is represented in terms of the levelised cost of electricity (*LCOE*), calculated according to Eq. (12) [56–58]. The levelised cost of CO_2 capture from air (LCOA) is defined in Eq. (13). These equations are based on the assumption that the capital and operating costs of the proposed process are completely covered by either electricity price or carbon tax alone. Therefore, the levelised cost of electricity and levelised cost of CO_2 capture from air indicate the minimum electricity price and carbon tax, respectively, for which the system breaks even without ascribing a value to the other product.

$$LCOE = \frac{TCR \times FCF + FOM}{8760 \dot{W}_{net} CF} + \frac{SFC}{\eta_{th}} + VOM \tag{12}$$

$$LCOA = \frac{TCR \times FCF + FOM + SFC}{8760 \dot{m}_{CO_2} CF} + VOM \tag{13}$$

These parameters correlate thermodynamic performance indicators, such as net power output, net thermal efficiency, rate at which CO_2 is removed from the atmosphere, and capacity factor (*CF*), with economic performance indicators, such as total capital requirement (*TCR*), variable (*VOM*) and fixed (*FOM*) operating and maintenance costs, specific fuel cost (*SFC*), and the fixed charge factor (*FCF*), which considers the system's lifetime and project interest rate.

Table 2: Capital cost estimation and economic model assumptions

Equipment [Scaling parameter]	Correlation
Solid-oxide fuel cell stack [Active area, AC_{SOFC} (m^2); Operating temperature, T_{SOFC} (K) [59]]	$C_{SOFC} = AC_{SOFC}(2.96T_{SOFC} - 1907)$
DC-to-AC inverter [Rated power output, $\dot{W}_{SOFC,DC}$ (kW) [59]]	$C_{SOFC,DC/AC} = 1e5\left(\frac{\dot{W}_{SOFC,DC}}{500}\right)^{0.7}$
Solid-oxide fuel cell auxiliaries [Stack cost, C_{SOFC} (USD) [59]]	$C_{SOFC,aux} = 0.1C_{SOFC}$
Fuel compressor [Break power requirement, $\dot{W}_{FC,BRK}$ (kW) [59,60]]	$C_{FC} = 91562\left(\frac{\dot{W}_{FC,BRK}}{445}\right)^{0.67}$
Air compressor [Break power requirement, $\dot{W}_{AC,BRK}$ (kW) [59,60]]	$C_{AC} = 91562\left(\frac{\dot{W}_{AC,BRK}}{445}\right)^{0.67}$
Fuel preheater [Heat exchange area, AC_{FPH} (m^2) [60]]	$C_{FPH} = 130\left(\frac{AC_{FPH}}{0.093}\right)$
Oxygen preheater [Heat exchange area, AC_{OXPH} (m^2) [60]]	$C_{OXPH} = 130\left(\frac{AC_{OXPH}}{0.093}\right)$
Air preheater 1 [Heat exchange area, AC_{APH1} (m^2) [60]]	$C_{APH1} = 130\left(\frac{AC_{APH1}}{0.093}\right)$
Air preheater 2 [Heat exchange area, AC_{APH2} (m^2) [59]]	$C_{APH2} = 2290(AC_{APH2})^{0.6}$
Steam turbine [Break power output, $\dot{W}_{ST,BRK}$ (kW) [61]]	$C_{ST} = 3744.3(\dot{W}_{ST,BRK})^{0.7} - 61.3(\dot{W}_{ST,BRK})^{0.95}$
Generator [Break power output, $\dot{W}_{ST,BRK}$ (kW) [61]]	$C_{GEN} = 26.18(\dot{W}_{ST,BRK})^{0.95}$
Boiler feedwater pump [Break power output, $\dot{W}_{BFP,BRK}$ (kW); Isentropic efficiency, η_{BFP} (-) [62]]	$C_{BFP} = 623.22(\dot{W}_{BFP,BRK})^{0.95}\left(1 + \frac{0.2}{1 - \eta_{BFP}}\right)$
Heat recovery steam generator [Heat transferred in evaporator, $\dot{Q}_{EVA}$ (kW); Heat transferred in economiser, $\dot{Q}_{ECO}$ (kW); Log mean temperature difference in evaporator $\Delta T_{LMTD,EVA}$ (K); Log mean temperature difference in economiser, $\Delta T_{LMTD,ECO}$ (K); Steam generation rate, $\dot{m}_{steam}$ (kg/s); Gas flow rate, $\dot{m}_{gas}$ (kg/s) [60]]	$C_{HRSG} = 6570\left[\left(\frac{\dot{Q}_{EVA}}{\Delta T_{LMTD,EVA}}\right)^{0.8} + \left(\frac{\dot{Q}_{ECO}}{\Delta T_{LMTD,ECO}}\right)^{0.8}\right] + 21276\dot{m}_{steam} + 1184.4(\dot{m}_{gas})^{0.95}$
Condenser [Heat exchange area, AC_{COND} (m^2) [63]]	$C_{COND} = 8500 + 490(AC_{COND})^{0.85}$
Air separation unit [O_2 production rate, $\dot{m}_{O2}$ (kg/s) [64]]	$C_{ASU} = 2.926e5\left(\frac{\dot{m}_{O_2}}{28.9}\right)^{0.7}$
CO_2 compression unit [Break power requirement, $\dot{W}_{CCU}$ (kW) [65]]	$C_{CCU} = 1.22914e7\left(\frac{\dot{W}_{CCU,BRK}}{13000}\right)^{0.67}$
Calciner [Material production rate, $\dot{m}_{calc}$ (kg/s) [66]]	$C_{calc} = 1.30523e8\left(\frac{\dot{m}_{calc}}{344.24}\right)^{0.7}$

The capital cost was determined from the capital cost correlations for each unit, which were taken from the literature and are gathered in Table 2. These correlations have been selected from the literature studies that analysed systems of comparable scale (2–60 $MW_{el,DC}$) and are based on the exponential method function. Such approach to cost estimation considers the effect of the system scale on the capital cost [67]. Fixed and variable operating and maintenance costs are calculated as a fraction of total capital cost, while operating costs associated with fuel and sorbent consumption, CO_2 transport and storage, and CO_2 emission are determined based on process simulation outputs using economic data from Table 3.

Table 3: Economic model assumptions

Parameter	Value
Variable operating cost as a fraction of total capital cost (%) [58,68]	2.0
Fixed operating cost as a fraction of total capital cost (%) [58,68]	1.0
Carbon tax (£/tCO_2) [58,68]	0.0
Limestone cost (£/t) [58,68,69]	6.0
Dolomite cost (£/t) [69]	6.0
Magnesite cost (£/t) [70]	140
CO_2 transport and storage cost (£/tCO_2) [71]	7.0
Natural gas price (£/GJ) [67]	3.0
Expected lifetime (years) [58,68]	25
Project interest rate (%) [58,68]	8.78
Capacity factor (%) [58,68]	80
USD/GBP exchange ratio (-)	0.8

3.2 Thermo-economic performance evaluation

The analysis of thermodynamic performance of the proposed process (Table 4) revealed that it can deliver a net power output between 19.5 and 21.3 MW_{el} at a net thermal efficiency of 43.7 and 47.7$\%_{LHV}$, respectively, depending on the kind of fresh material fed to the flash calciner. Such performance falls between the figures reported for supercritical coal-fired power plants (40–46$\%_{LHV}$) and natural gas combined cycle power plants (53$\%_{LHV}$) [72]. Although the estimated net thermal efficiencies are lower than figures reported for hybrid systems comprising a SOFC and gas turbine (~70$\%_{LHV}$) [44,45], the proposed process produces a concentrated CO_2 stream, which has been purified and conditioned for transport and storage, and calcined material that is used for CO_2 capture from air. Therefore, not only does the proposed process operate with a net thermal efficiency comparable to conventional fossil fuel power generation systems, it also can become a negative emitter of CO_2, having the potential to remove 463.5–882.3 $gCO_2/kW_{el}h$. Importantly, this study only considers the reaction of the calcined material with CO_2 on direct contact with air over an elongated period of time to form carbonated material. If the calcined material was dissolved in seawater, an additional CO_2 drawdown could be achieved as it would form a bicarbonate material. This would increase the CO_2 uptake from air by a factor of 1.6–1.8 [73–76]. However, such an approach may bring potential environmental hazards, leading to an increased regulatory burden and governance issues [73,74]. In addition, the concentrated CO_2 stream (>98%$_{vol}$ CO_2) resulting from the SOFC and the calciner is generated at a rate varying between 886.6 and 1345.5 $gCO_2/kW_{el}h$ for the system using limestone and magnesite, respectively.

Table 4: Key techno-economic performance indicators under initial design basis[†]

Parameter	Limestone (at 900°C)	Dolomite (at 850°C)	Dolomite (at 550°C)	Magnesite (at 550°C)
Thermodynamic performance indicators				
Solid-oxide fuel cell gross power output (MW_{el})	23.0	23.0	23.0	23.0
Steam cycle gross power output (MW_{el})	1.2	1.1	0.1	0.1
Parasitic load (MW_{el})	2.9	3.1	3.2	3.6
Net power output (MW_{el})	21.3	21.0	19.9	19.5
Net thermal efficiency ($\%_{LHV}$)	47.7	47.0	44.5	43.7
Calcined material production rate (t/d)	307.4	311.0	1112.9	447.7
Specific negative CO_2 emission ($g/kW_{el}h$)	463.5	556.2	662.2	882.3
CO_2 sequestered from solid-oxide fuel cell ($g/kW_{el}h$)	321.2	326.3	344.2	351.3
CO_2 sequestered from calciner ($g/kW_{el}h$)	565.5	659.9	771.7	994.2
Total CO_2 sequestered ($g/kW_{el}h$)	886.6	986.2	1116.0	1345.5
Economic performance indicators				
Specific capital cost ($£/kW_{el,gross}$)	1397.9	1412.7	1740.5	1529.3
Specific capital cost ($£/kW_{el,net}$)	1589.9	1620.9	2023.1	1811.0
Levelised cost of electricity[a] ($£/MW_{el}h$)	69.1	71.8	99.6	325.4
Levelised cost of CO_2 capture from air[b] ($£/tCO_2$)	149.0	129.1	150.5	368.8
Levelised cost of CO_2 capture from air[c] ($£/tCO_2$)	41.2	39.2	74.9	312.1

[a]Assuming all costs are covered by electricity
[b]Assuming all costs are covered by carbon tax
[c]Assuming the levelised cost of electricity is 50 $£/MW_{el}h$

Having assessed the impact of the type of fresh material used in the calciner, the systems using limestone and magnesite were shown to yield the highest and the

[†] The detailed calculations of the net thermal efficiency of the proposed process are available in the Appendix B.

lowest net power output, respectively. The systems using dolomite yielded net power outputs that fell between these. The main causes of poorer thermodynamic performance of the systems using dolomite and magnesite were increased parasitic load, which can be primarily associated with higher calcined material production rates and thus more CO_2 fed to the CCU, and less heat available for recovery in the saturated steam cycle. Importantly, the calcination of dolomite was considered at 850 and 550°C, leading to complete or partial conversion of the fresh material, respectively. As $CaCO_3$ was not calcined at 550°C, the calcined material production rate for the latter case was 3.6 times higher than for the system using limestone or dolomite at 850°C. Nevertheless, due to a large amount of inert material (57.5%$_{wt}$ $CaCO_3$) needed to be preheated to the calciner operating temperature, the CO_2/H_2O stream left the calciner at 216°C, which is below the steam saturation temperature at 40 bar (250°C). Therefore, the steam was raised at 5 bar in this case, leading to a marginal contribution of the saturated steam cycle to the net power output of the proposed process. It is important to note that an increase in the amount of fresh material processed in the calciner was allowed by a reduction of the calcination temperature, as more heat became available for calcination. However, this reduced the amount of heat available for saturated steam generation, revealing the trade-off between the net power output and the calcined material production rate, hence the specific negative CO_2 emissions. Therefore, for the calciner operating at 550°C, the saturated steam cycle made a very low contribution to the net power output of the entire process. As a result, it is not thermodynamically substantiated at low calcination temperatures.

The economic assessment (Table 4) of the proposed process revealed that its specific capital cost would vary between 1397.9 and 1740.5 £/kW$_{el,gross}$. It needs to be stressed, however, that such specific capital cost is higher than figures reported for natural gas combined cycle power plants (400–700 £/kW$_{el,gross}$) and coal-fired power plants (1000–1300 £/kW$_{el,gross}$) [49,77], which is mainly because of the high specific capital cost of the SOFC, approximately 900–1000 £/kW$_{el,gross}$ [45], accounting for 50–70% of the capital cost estimated for the proposed process. Nevertheless, such capital cost compares favourably with that for integrated gasification combined cycle power plants (1300–2100 £/kW$_{el,gross}$), natural gas combined cycle power plants with CO_2 capture (730–1010 £/kW$_{el,gross}$, and coal-fired power plants with CO_2 capture (1700–2300 £/kW$_{el,gross}$) [49,77], making the proposed process economically competitive.

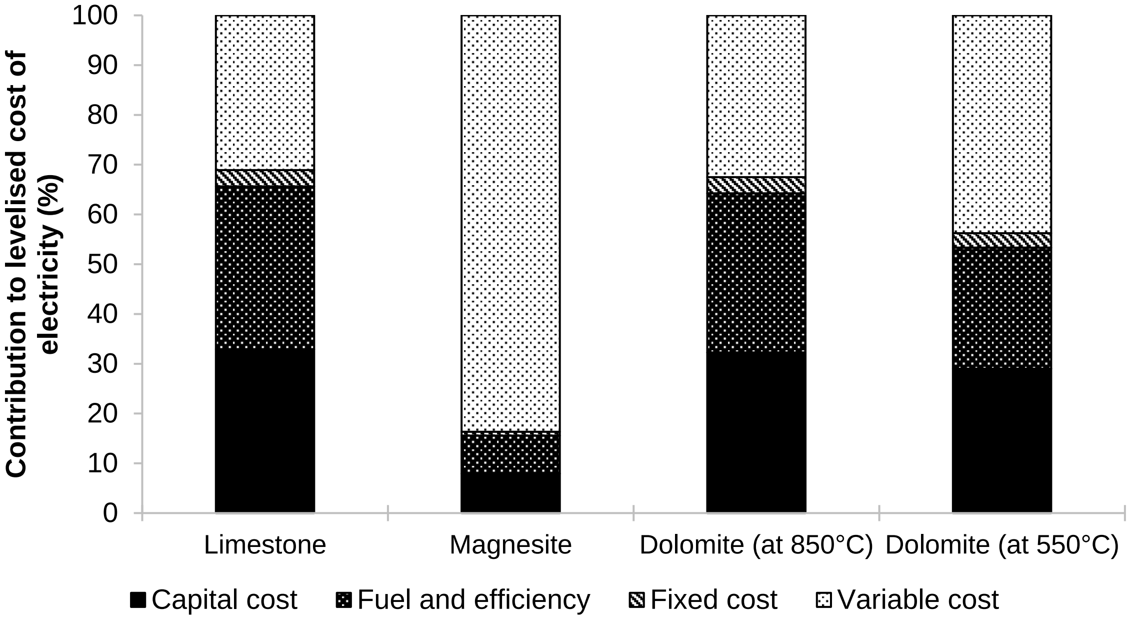

Figure 3: Distribution of the components of the levelised cost of electricity

Assuming that the capital and operating costs of the proposed process are only covered by electricity, the LCOE was estimated to vary between 69.1 and 325.4 £/MW$_{el}$h for the system using limestone and magnesite, respectively. As shown in Figure 3, the main cause behind such difference in the estimated LCOE arises from the variable cost component, the contribution of which is significantly higher in the system using magnesite (83.6%) compared to the system using limestone (31.1%).

This can be associated primarily with a significant difference in the limestone (6 £/t) and magnesite (140 £/t) cost and higher calcined material production rate for the latter system. Therefore, to reduce the consumption of fresh magnesite, it may be more feasible to consider a closed-loop regenerative process. The LCOE for the system using dolomite was found to vary between 71.8 (850°C) and 99.6 £/MW$_{el}$h (550°C). The LCOE distribution of the former system is comparable to that of the system using limestone, with a contribution of the variable cost higher by 1.4% points. On the other hand, an increase in the LCOE estimated for the latter system is associated primarily with a considerably higher calcined material production rate that is reflected in increased contributions of both capital cost (23.2 £/MW$_{el}$h) and variable cost (23.0 £/MW$_{el}$h) that were 1.9 and 1.6% higher, respectively, compared with the system using limestone. Nevertheless, the LCOE of the proposed process (limestone or dolomite only) was found to fall between figures reported for fossil fuels power plants without (28–55 £/MW$_{el}$h) and with CO_2 capture (39–78 £/MW$_{el}$h) [77,78]. It would also be competitive to the LCOE reported for other dispatchable technologies, such as advanced nuclear power plants, geothermal, and biomass power plants, as well as non-dispatchable technologies, such as wind, solar, and hydroelectric [78] (Figure 4). Therefore, the proposed process can be economically competitive, even with no price associated with the CO_2 capture.

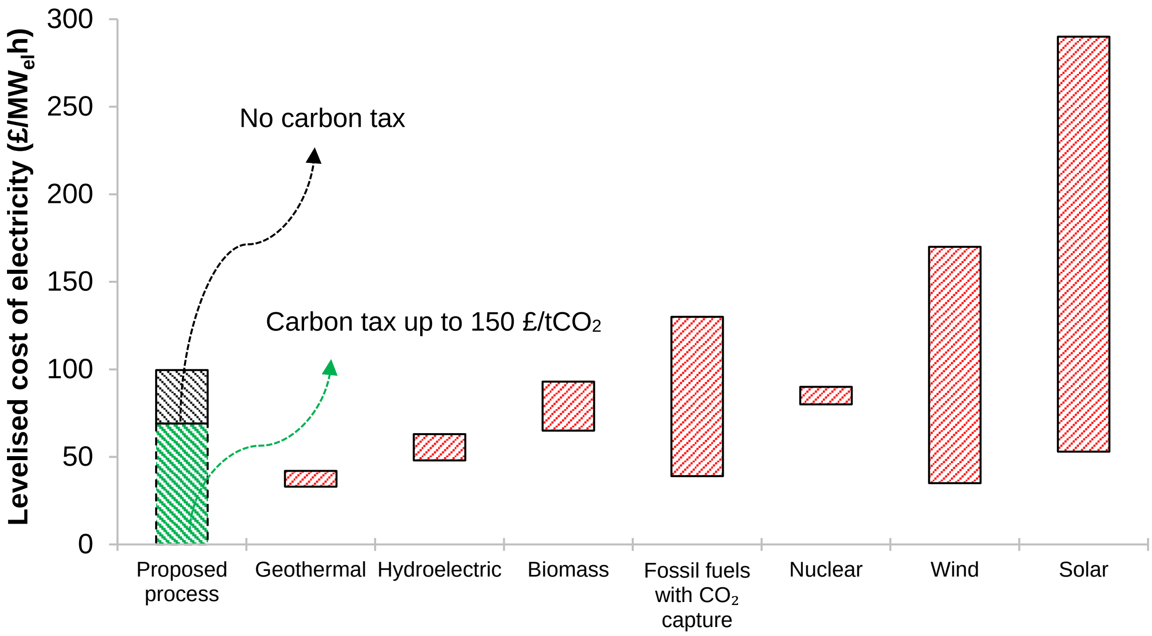

Figure 4: Levelised cost of electricity comparison between the process for simultaneous power generation and direct CO_2 removal from the air (this study, limestone and dolomite only), and low-carbon power generation technologies [78]

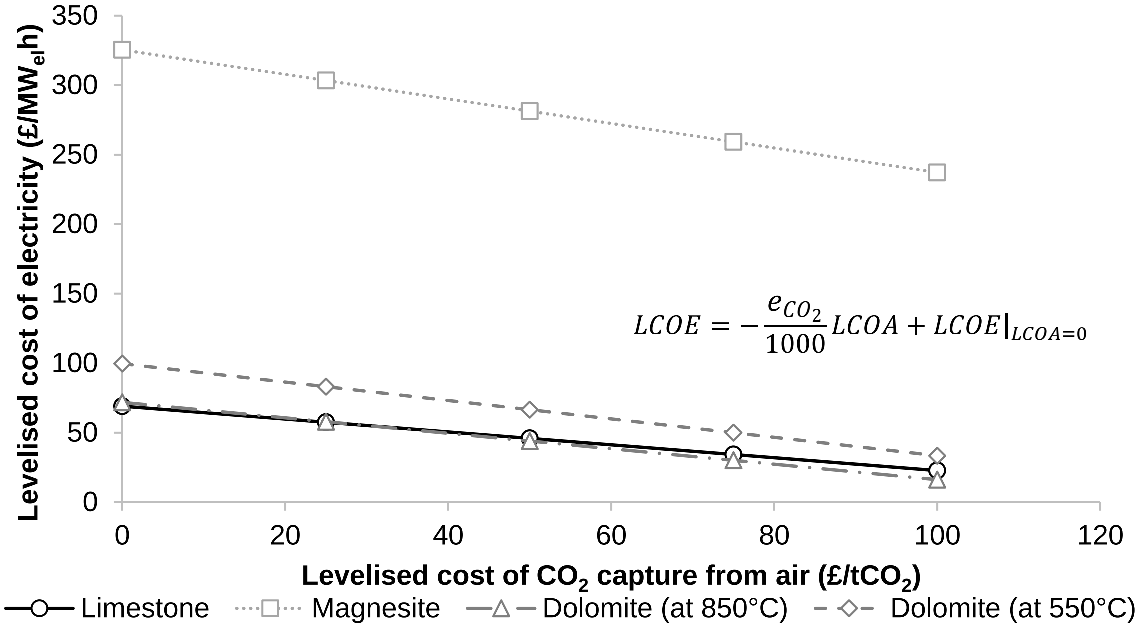

Figure 5: Correlation between levelised cost of CO_2 capture from air and levelised cost of electricity

Importantly, it is expected that the proposed process will operate with specific negative CO_2 emissions varying between 463.5 g/kW$_{el}$h (limestone) and 882.3 g/kW$_{el}$h (magnesite), assuming that the calcined material will be completely carbonated over time. Therefore, if CO_2 emissions to the atmosphere will become penalised by a carbon tax, the system operating with negative CO_2 emissions will make a profit from removing CO_2 directly from the air. As a result, the LCOE would be reduced as the capital and operating costs would be subsidised by the income from CO_2 removed from the air. The economic assessment (Table 4) has indicated that the LCOE will become zero, which implies that the process will make revenue regardless of the price of electricity on the market, if the LCOA varies between 129.1 £/tCO_2 (dolomite at 850°C) and 368.8 £/tCO_2 (magnesite), which are lower than 400–800 £/tCO_2 reported for other DAC processes [12,13]. Yet, the LCOA is expected to increase with reduction of the carbonation extent. Nevertheless, the dependence between these economic performance indicators was found to be linear (Figure 5) with the slope equal to the specific CO_2 emissions and the constant term equal to the LCOE at no cost associated with CO_2 capture from the air. Analysis of such a correlation for different types of fresh material indicated that although the LCOE is lowest for the system using limestone, this system will not become more beneficial at high LCOE, and thus at higher rates of carbon tax. This is a result of higher specific negative emissions of the system using dolomite compared to the system using limestone. Importantly, the LCOE for the system using magnesite would be higher than for other material types, unless the LCOA reaches values above 647.6 £/tCO_2. Therefore, the high cost of magnesite makes its use in the once-through system impractical, regardless of the highest specific negative CO_2 emission. Nevertheless, for the remaining systems to achieve a reasonable LCOE of 50 £/MW_{el}h, the carbon tax should be between 39.2 and 74.9 £/tCO_2.

As stated above, the DAC concepts are expected to be deployed only after 2050, by which time the centralised CO_2 emitters will have been completely decarbonised

[17,18]. This is mostly because of their unfavourable economics compared to CO_2 capture from flue gases that contain much higher CO_2 concentrations. However, because of the capability to remove CO_2 from the air, the proposed system is capable of alleviating emissions from distributed sources in agriculture, buildings and transportation sectors that cannot be easily mitigated in any other way. As the proposed concept combines high-efficiency power generation and CO_2 capture from the air, the capital and operating costs can be met by both electricity sales and carbon tax. Therefore, depending on the market conditions, the proposed process can be seen as a flexible solution that is able to generate profit either from electricity sales or negative CO_2 emissions.

3.3 Parametric study

The thermodynamic performance of the proposed process is directly dependent upon the performance of the SOFC, as it is the main source of heat and power in this process. Therefore, a parametric study (Figure 6) has been performed to assess the effect of the key design conditions of the SOFC, such as steam-to-carbon ratio, fuel utilisation and current density, on performance of the entire process. Figure 6 shows that the thermodynamic performance of the process is not sensitive to the S/C ratio, but the optimum operating point can be observed for figures between 2.5 and 3.5, across all key performance indicators considered. Importantly, reduction in fuel utilisation caused reduction in the net thermal efficiency of the entire process (Figure 6a), which can be associated mostly with less power generated in the SOFC and higher O_2 requirement to complete the fuel combustion in the calciner. However, this resulted in more heat available for calcination, resulting in higher calcined material production rates (Figure 6b). This, in turn, results in higher specific negative CO_2 emissions (Figure 6c). Conversely, reduction in the current density will increase the net thermal efficiency (Figure 6a), as a result of lower voltage losses. This, in turn, reduces the amount of heat available for the calcination, and thus the amount of calcined material (Figure 6b) and potential specific negative CO_2 emissions (Figure 6c). Although operating the SOFC at lower fuel utilisation and higher current density will lead to a higher LCOE, such operating conditions are expected to lead to reduction in the LCOA.

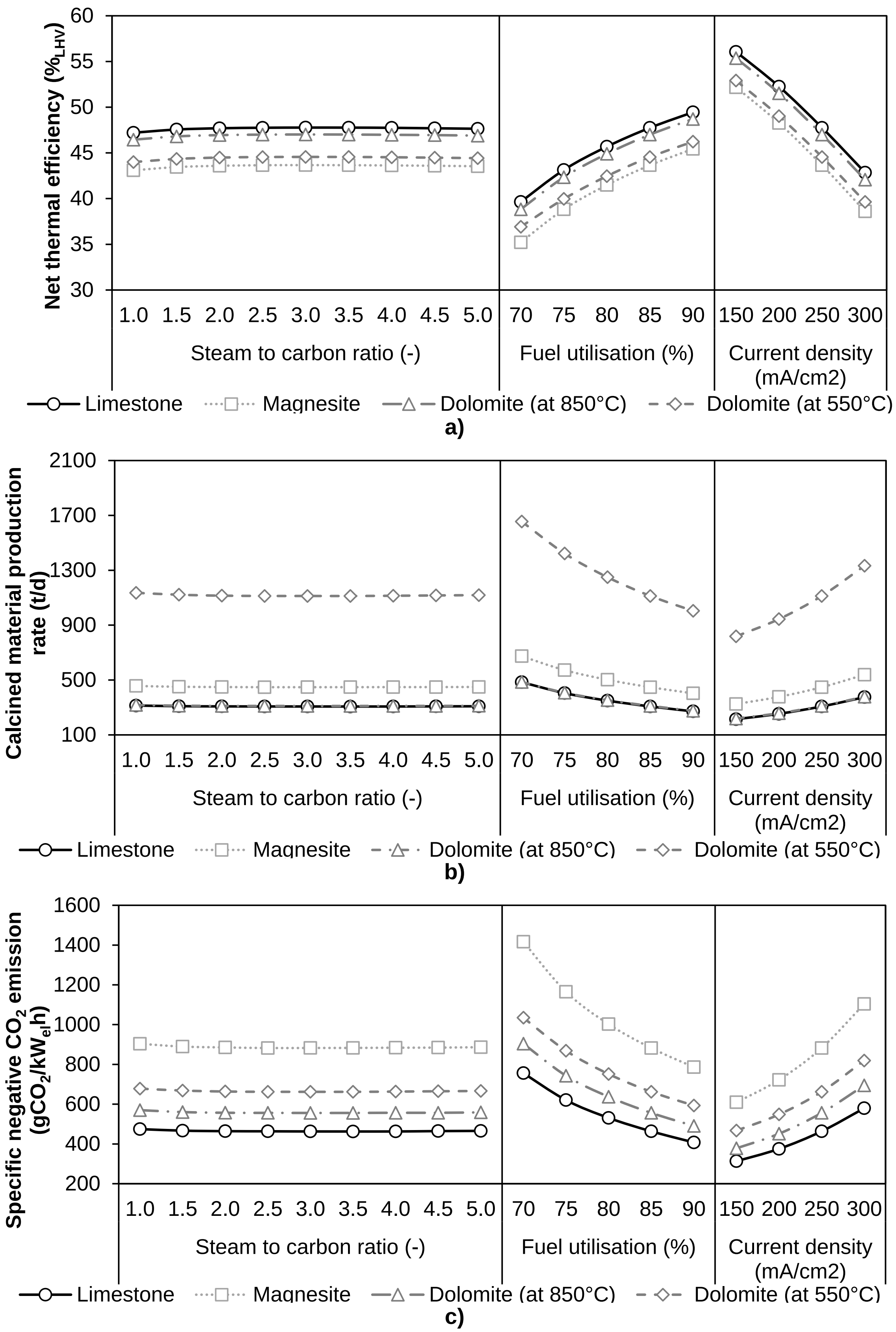

Figure 6: Effect of key solid-oxide fuel cell operating conditions on key thermodynamic performance indicators

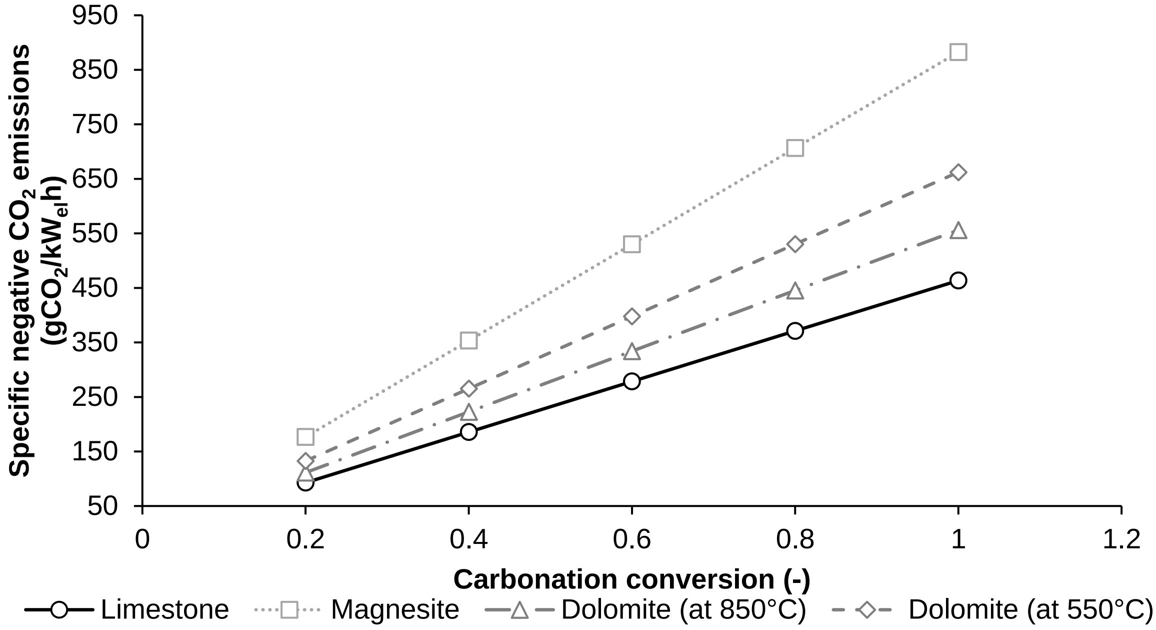

a)

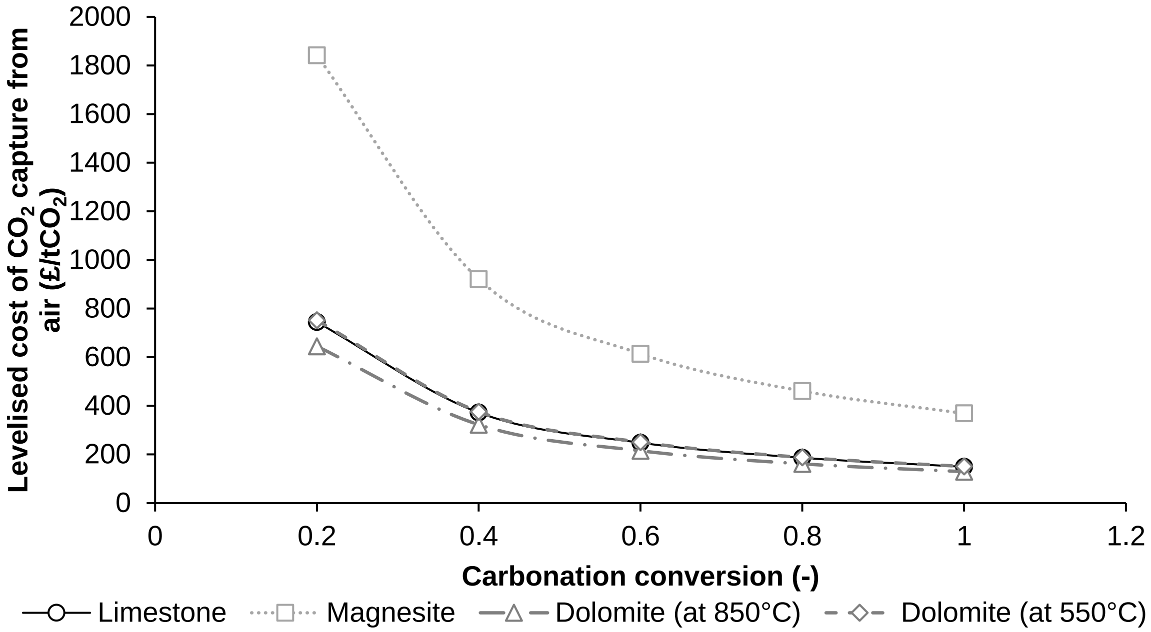

b)

Figure 7: Effect of carbonation conversion on a) specific negative CO_2 emissions and b) levelised cost of CO_2 capture from air assuming all costs are covered by carbon tax

In the analysis conducted thus far it was assumed that the calcined material is completely carbonated when exposed to the ambient air. However, it is uncertain whether this will, in fact, be achieved. For this reason, the effect of carbonation conversion on the specific negative CO_2 emissions and LCOA has been assessed (Figure 7). As expected, reduction in the carbonation conversion results in lowered specific negative CO_2 emissions (Figure 7a). This, along with the speculations made in Section 3.2, led to subsequent increase in the LCOA (Figure 7b). This figure can increase to between 1842.1 £/tCO_2 (magnesite) and 644.9 £/tCO_2 (dolomite at 850°C), considering a carbonation conversion of 20% that is commonly used in evaluating the calcium looping process [22,72,79]. Such values of the LCOA (limestone or dolomite only) fall in the middle of the 400–800 £/tCO_2 range reported for other DAC processes [12,13]. Nevertheless, as higher carbonation conversions could be expected to be achieved over an elongated period of time, the proposed process is expected to be more economically favoured compared to the other DAC processes. To gather more profound insight into the techno-economic performance and to arrive at the optimal operating conditions of the proposed process, a probabilistic framework needs to be employed to account for process uncertainties [80,81]. Furthermore, the feasibility of using a closed-loop regenerative process needs to be evaluated, especially for the system using magnesite. Yet, this is outside of this study scope.

4 CONCLUSIONS

This study assessed the techno-economic feasibility of a process for simultaneous power generation and CO_2 removal from the air. To assess the thermodynamic and economic performance of the proposed process, a process model, which comprises a fresh material calciner, heat recovery system including a simple steam cycle, CO_2 compression unit, and SOFC, was developed in Aspen Plus®.

The thermodynamic performance of the proposed system was found to be dependent upon the type of fresh material fed to the carbonator. Namely, under initial design conditions, the net thermal efficiency varied between 43.7 (magnesite) and 47.7%$_{LHV}$ (limestone), and the corresponding potential specific negative CO_2 emissions were 882.3 and 463.5 gCO_2/kW$_{el}$h, respectively. The thermodynamic performance of the system using dolomite fell between these figures. The main benefits of the proposed process are, therefore, high efficiency of power generation, which is comparable to conventional fossil fuel power generation systems, with simultaneous production of a concentrated CO_2 stream (>98%$_{vol}$ CO_2) and capability to remove CO_2 directly from the air.

The economic assessment of the proposed process revealed that its specific capital cost is higher than figures reported for conventional fossil fuel power systems, but lower than that for integrated gasification combined cycle power plants and coal-fired power plants with CO_2 capture. Under initial design conditions, the LCOE was found to vary between 69.1 (limestone) and 325.4 £/MW$_{el}$h (magnesite), while the LCOA varied between 368.8 (magnesite) and 129.1 £/tCO_2 (dolomite at 850°C), which is lower than for other DAC concepts. Therefore, depending on the market conditions, the proposed process can make a profit either from electricity sales or negative CO_2 emissions (carbon tax). Importantly, the techno-economic analysis indicated that limestone should be the favoured material for the former case, and dolomite for the latter.

The parametric study indicated that the performance of the proposed process is highly dependent upon the fuel utilisation and current density in the SOFC. Although operating the SOFC at lower fuel utilisation and higher current density will lead to a higher LCOE, such operating conditions are expected to lead to reduction in the LCOA. Moreover, it is uncertain whether complete carbonation conversion will be achieved, which would affect the specific negative CO_2 emissions and LCOA. However, the parametric study showed that even with 20% carbonation conversion, the LCOA will fall in the middle of the range reported for other DAC concepts. Nevertheless, it is suggested that probabilistic assessment of the techno-economic performance and optimisation of the proposed process should be conducted. Furthermore, the feasibility of using a closed-loop regenerative process needs to be evaluated, especially for the system using magnesite.

ACKNOWLEDGEMENTS

This publication is based on research conducted within the “Balanced Energy Network” project supported by InnovateUK Integrated Supply Chains for Energy Systems Grant (InnovateUK reference: 102624). The consortium consists of ICAX Ltd. (project lead coordinators), London South Bank University, Terra Firma Ground Investigations Ltd., Upside Energy Ltd., Mixergy Ltd., Origen Power Ltd., and Cranfield University. The authors are grateful for their support and input.

APPENDIX A

In evaluating the validity of the SOFC process model developed in Aspen Plus® for the purpose of this study, the operating conditions were selected according to a description provided by Zhang et al. [47]. The process model was stress-tested using different SOFC characteristics available in the Fuel Cell Handbook [55]. As shown in Table A, the prediction of the developed process model closely reflects the performance reported in the literature.

Table A: Validation of the solid-oxide fuel cell process model

Parameter	Literature data [82–84]	Literature [47]	Literature [85]	Model - Curve 1*	Model - Curve 2#
Fuel utilisation (%)	0.85	0.85	0.85	0.85	0.85
Voltage (mV)	N/A	700	683.0	703.7	623.0
Current density (mA/cm^2)	180	178	182.9	177.4	200.3
Pre-reforming temperature (°C)	550	536	535.1	536.0	536.0
Pre-reformer CH_4 conversion (%)	10-15	25.9	25.0	25.9	26.1
Cathode inlet temperature (°C)	N/A	821.3	823.7	823.5	823.5
Combustion products temperature (°C)	N/A	1012.4	1012.3	1012.0	1012.0
Stack exhaust temperature (°C)	847	833.85	833.7	833.5	833.5
Anode inlet gas composition (%$_{vol}$)	N/A	27.9% H_2O, 23.1% CO_2, 27% H_2, 5.6% CO, 10.1% CH_4, 6.2% N_2	27.8% H_2O, 23.1% CO_2, 26.9% H_2, 5.6% CO, 10.4% CH_4, 6.2% N_2	27.8% H_2O, 23.1% CO_2, 27.2% H_2, 5.6% CO, 10.1% CH_4, 6.2% N_2	27.7% H_2O, 23.1% CO_2, 27.2% H_2, 5.7% CO, 10.1% CH_4, 6.2% N_2
Anode exhaust gas composition (%$_{vol}$)	48% H_2O, 28% CO_2, 14% H_2, 5% CO, 5% N_2	50.9% H_2O, 24.9% CO_2, 11.6% H_2, 7.4% CO, 5.1% N_2	50.9% H_2O, 24.9% CO_2, 11.6% H_2, 7.4% CO, 5.1% N_2	50.9% H_2O, 25.0% CO_2, 11.6% H_2, 7.4% CO, 5.1% N_2	50.9% H_2O, 25.0% CO_2, 11.6% H_2, 7.4% CO, 5.1% N_2
Cathode exhaust gas composition (%$_{vol}$)	N/A	17.7% O_2, 82.3% N_2	17.7% O_2, 82.3% N_2	17.7% O_2, 82.3% N_2	17.7% O_2, 82.3% N_2
Stack exhaust gas composition (%$_{vol}$)	5% H_2O, 2% CO_2, 16% O_2, 77% N_2	4.5% H_2O, 2.3% CO_2, 15.9% O_2, 77.3% N_2	4.5% H_2O, 2.3% CO_2, 15.9% O_2, 77.3% N_2	4.5% H_2O, 2.3% CO_2, 15.9% O_2, 77.3% N_2	4.5% H_2O, 2.3% CO_2, 15.9% O_2, 77.3% N_2
DC power output (kW)	120	120	120	120	120
AC efficiency (%$_{LHV}$)	50	52	51.28	52.8	46.8

*The solid-oxide fuel cell characteristics according to Figure 7.12 from Fuel Cell Handbook [55]

#The solid-oxide fuel cell characteristics according to Figure 7.17 from Fuel Cell Handbook [55]

APPENDIX B

Table B: Overall energy balance of the proposed process under the initial design basis

Parameter	Limestone (at 900°C)	Dolomite (at 850°C)	Dolomite (at 550°C)	Magnesite (at 550°C)
System energy input				
Fuel consumption rate (kg/s)	0.947	0.947	0.947	0.947
Lower heating value (MJ/kg)	47.206	47.206	47.206	47.206
Heat input (MW_{th})	44.690	44.690	44.690	44.690
Auxiliary equipment power requirement				
Air compressor ($MW_{el, AC}$)	0.493	0.494	0.505	0.493
Fuel compressor ($MW_{el, AC}$)	0.225	0.225	0.225	0.225
CO_2 compressor ($MW_{el, AC}$)	1.751	1.914	2.051	2.417
CO_2 pump ($MW_{el, AC}$)	0.034	0.037	0.039	0.046
Boiler feedweater pump ($MW_{el, AC}$)	0.009	0.008	0.000	0.001
Cooling water pump ($MW_{el, AC}$)	0.009	0.007	0.001	0.001
Air separation unit ($MW_{el, AC}$)	0.410	0.410	0.410	0.410
System power output				
Fuel cell gross power output ($MW_{el, AC}$)	23.000	23.000	23.000	23.000
Steam cycle gross power output ($MW_{el, AC}$)	1.270	1.098	0.136	0.100
Gross power output of the entire system ($MW_{el, AC}$)	24.270	24.098	23.136	23.100
Total auxiliary equipment power requirement ($MW_{el, AC}$)	2.931	3.095	3.231	3.592
Net power output of the entire system ($MW_{el, AC}$)	21.340	21.003	19.905	19.508
Net thermal efficiency of solid oxide fuel cell ($\%_{LHV}$)	49.859	49.857	49.839	49.859
Gross thermal efficiency of the entire system ($\%_{LHV}$)	54.308	53.924	51.776	51.690
Net thermal efficiency of the entire system ($\%_{LHV}$)	47.751	46.998	44.545	43.652

REFERENCES

[1] UN, 2015, *Adoption of the Paris Agreement*, United Nations Framework Convenction on Climate Change, Paris, France.

[2] H. J. Buck, 2016, “Rapid scale-up of negative emissions technologies: social barriers and social implications,” *Clim. Change*, 139, 2, 155–167.

[3] P. Smith, 2016, “Soil carbon sequestration and biochar as negative emission technologies,” *Glob. Chang. Biol.*, 22, 3, 1315–1324.

[4] J. Edmonds, P. Luckow, K. Calvin, M. Wise, J. Dooley, P. Kyle, S. H. Kim, P. Patel, and L. Clarke, 2013, “Can radiative forcing be limited to 2.6 Wm^{-2} without negative emissions from bioenergy and CO_2 capture and storage?,” *Clim. Change*, 118, 1, 29–43.

[5] IPCC, 2014, *Climate Change 2014: Mitigation of Climate Change*, Cambridge University Press, Cambridge, UK and New York, NY, USA.

[6] D. L. Sanchez and D. S. Callaway, 2016, “Optimal scale of carbon-negative energy facilities,” *Appl. Energy*, 170, 437–444.

[7] K. S. Lackner, S. Brennan, J. M. Matter, A.-H. A. Park, A. Wright, and B. van der Zwaan, 2012, “The urgency of the development of CO_2 capture from ambient air,” *Proc. Natl. Acad. Sci.* , 109, 33, 13156–13162.

[8] E. S. Sanz-Pérez, C. R. Murdock, S. A. Didas, and C. W. Jones, 2016, “Direct capture of CO_2 from ambient air,” *Chem. Rev.*, 19, 11840–11876.

[9] J. A. Wurzbacher, C. Gebald, S. Brunner, and A. Steinfeld, 2016, “Heat and mass transfer of temperature-vacuum swing desorption for CO_2 capture from air,” *Chem. Eng. J.*, 283, 1329–1338.

[10] L. A. Darunte, A. D. Oetomo, K. S. Walton, D. S. Sholl, and C. W. Jones, 2016, “Direct air capture of CO_2 using amine functionalized MIL-101(Cr),” *ACS Sustain. Chem. Eng.*, 4, 10, 5761–5768.

[11] A. Goeppert, M. Czaun, G. K. Surya Prakash, and G. A. Olah, 2012, “Air as the renewable carbon source of the future: an overview of CO_2 capture from the atmosphere,” *Energy Environ. Sci.*, 5, 7, 7833–7853.

[12] D. W. Keith, M. Ha-Duong, and J. K. Stolaroff, 2006, “Climate strategy with CO_2 capture from the air,” *Clim. Change*, 74, 1–3, 17–45.

[13] K. Z. House, A. C. Baclig, M. Ranjan, E. A. van Nierop, J. Wilcox, and H. J. Herzog, 2011, “Economic and energetic analysis of capturing CO_2 from ambient air,” *Proc. Natl. Acad. Sci.*, 108, 51, 20428–20433.

[14] E. S. Rubin, J. E. Davison, and H. J. Herzog, 2015, “The cost of CO_2 capture and storage,” *Int. J. Greenh. Gas Control*, 40, 378–400.

[15] R. Socolow, M. Desmond, R. Aines, J. Blackstock, O. Bolland, T. Kaarsberg, N. Lewis, M. Mazzotti, A. Pfeffer, K. Sawyer, J. Siirola, B. Smit, and J. Wilcox, 2011, *Direct air capture of CO_2 with chemicals: A technology assessment for the APS panel on public affairs*, American Physical Society, Ridge, NY, USA.

[16] D. W. Keith, 2009, “Why capture CO_2 from the atmosphere?,” *Science*, 325,

5948, 1654–1655.

[17] J. Gale, 2012, *Direct air capture - an update*, IEA Greenhouse Gas R&D Programme, Cheltenham, UK.

[18] J. Gale, 2015, *Status report on direct air capture*, IEA Greenhouse Gas R&D Programme, Cheltenham, UK.

[19] F. Zeman, 2007, "Energy and material balance of CO_2 capture from ambient air," *Environ. Sci. Technol.*, 41, 21, 7558–7563.

[20] D. W. Keith and M. Ha-Duong, 2002, "CO_2 capture from the air: Technology assessment and implications for climate policy," *Greenh. Gas Control Technol.* , 2, 187–197.

[21] R. Baker, 1973, "The reversibility of the reaction $CaCO_3 \rightleftarrows CaO+CO_2$," *J. Appl. Chem. Biotechnol.*, 23, 10, 733–742.

[22] D. P. Hanak, C. Biliyok, E. J. Anthony, and V. Manovic, 2015, "Modelling and comparison of calcium looping and chemical solvent scrubbing retrofits for CO_2 capture from coal-fired power plant," *Int. J. Greenh. Gas Control*, 42, 226–236.

[23] L. M. Romeo, J. C. Abanades, J. M. Escosa, J. Paño, A. Giménez, A. Sánchez-Biezma, and J. C. Ballesteros, 2008, "Oxyfuel carbonation/calcination cycle for low cost CO_2 capture in existing power plants," *Energy Convers. Manag.*, 49, 10, 2809–2814.

[24] J. Ströhle, A. Lasheras, A. Galloy, and B. Epple, 2009, "Simulation of the carbonate looping process for post-combustion CO_2 capture from a coal-fired power plant," *Chem. Eng. Technol.*, 32, 3, 435–442.

[25] J. C. Abanades, R. Murillo, J. R. Fernandez, G. Grasa, and I. Martinez, 2010, "New CO_2 capture process for hydrogen production combining Ca and Cu chemical loops," *Environ. Sci. Technol.*, 44, 17, 6901–6904.

[26] B. Duhoux, P. Mehrani, D. Y. Lu, R. T. Symonds, E. J. Anthony, and A. Macchi, 2016, "Combined calcium looping and chemical looping combustion for post-combustion carbon dioxide capture: process simulation and sensitivity analysis," *Energy Technol.*, 4, 1–14.

[27] D. C. Ozcan, A. Macchi, D. Y. Lu, A. M. Kierzkowska, H. Ahn, C. R. Müller, and S. Brandani, 2015, "Ca–Cu looping process for CO_2 capture from a power plant and its comparison with Ca-looping, oxy-combustion and amine-based CO_2 capture processes," *Int. J. Greenh. Gas Control*, 43, 198–212.

[28] V. Manovic and E. J. Anthony, 2011, "Integration of calcium and chemical looping combustion using composite CaO/CuO-based materials," *Environ. Sci. Technol.*, 45, 24, 10750–10756.

[29] I. Martínez, R. Murillo, G. Grasa, N. Rodríguez, and J. C. Abanades, 2011, "Conceptual design of a three fluidised beds combustion system capturing CO_2 with CaO," *Int. J. Greenh. Gas Control*, 5, 3, 498–504.

[30] J. C. Abanades, E. J. Anthony, J. Wang, and J. E. Oakey, 2005, "Fluidized bed combustion systems integrating CO_2 capture with CaO," *Environ. Sci. Technol.*, 39, 8, 2861–2866.

[31] H. Moon, H. Yoo, H. Seo, Y. K. Park, and H. H. Cho, 2015, "Thermal design of heat-exchangeable reactors using a dry-sorbent CO_2 capture multi-step process," *Energy*, 84, 704–713.

[32] M. Junk, M. Reitz, J. Strohle, and B. Epple, 2016, "Technical and economical assessment of the indirectly heated carbonate looping process," *J. Energy Resour. Technol.*, 138, 4.

[33] M. Junk, M. Reitz, J. Ströhle, and B. Epple, 2013, "Thermodynamic evaluation and cold flow model testing of an indirectly heated carbonate looping process," *Chem. Eng. Technol.*, 36, 9, 1479–1487.

[34] J. A. H. Oates, *Lime and limestone, chemistry and technology, production and uses*. Weinheim, Germany: Wiley–VCH, 1998.

[35] H. G. F. Winkler, *Petrogenesis of metamorphic rocks*. Berlin, Germany: Springer, 1976.

[36] M. Erans, V. Manovic, and E. J. Anthony, 2016, "Calcium looping sorbents for CO_2 capture," *Appl. Energy*, 180, 722–742.

[37] G. Itskos, P. Grammelis, F. Scala, H. Pawlak-Kruczek, A. Coppola, P. Salatino, and E. Kakaras, 2013, "A comparative characterization study of Ca-looping natural sorbents," *Appl. Energy*, 108, 373–382.

[38] J. M. Valverde, P. E. Sanchez-Jimenez, A. Perejon, and L. A. Perez-Maqueda, 2013, "Constant rate thermal analysis for enhancing the long-term CO_2 capture of CaO at Ca-looping conditions," *Appl. Energy*, 108, 108–120.

[39] C. Ortiz, J. M. Valverde, and R. Chacartegui, 2016, "Energy consumption for CO_2 capture by means of the calcium looping process: A comparative analysis using limestone, dolomite, and steel slag," *Energy Technol.*, 4, 10, 1317–1327.

[40] FuelCell Energy, 2015, "FuelCell Energy sells 8.4 MW more modules to its Korean partner," *Fuel Cells Bulletin*, 2015, 12, 6–7.

[41] S. Patel, "59-MW fuel cell park opening heralds robust global technology future," *Power*, 158, 5, 2014.

[42] O. Thomas, "World's Largest Fuel Cell Plant Opens in South Korea," *Power*, 2014.

[43] M. Andersson and B. Sundén, 2015, *Technology review – solid oxide fuel cell*, ENERGIFORSK, Stockholm, Sweden.

[44] M. Ameri and R. Mohammadi, 2013, "Simulation of an atmospheric SOFC and gas turbine hybrid system using Aspen Plus software," *Int. J. Energy Res.*, 37, 5, 412–425.

[45] A. V. Akkaya, 2007, "Electrochemical model for performance analysis of a tubular SOFC," *Int. J. Energy Res.*, 31, 1, 79–98.

[46] P. Aguiar, D. Chadwick, and L. Kershenbaum, 2004, "Effect of methane slippage on an indirect internal reforming solid oxide fuel cell," *Chem. Eng. Sci.*, 59, 1, 87–97.

[47] W. Zhang, E. Croiset, P. L. Douglas, M. W. Fowler, and E. Entchev, 2005, "Simulation of a tubular solid oxide fuel cell stack using AspenPlusTM unit

operation models," *Energy Convers. Manag.*, 46, 2, 181–196.

[48] Energy Institute, 2013, *Hazard analysis for offshore carbon capture platforms and offshore pipelines*, The Energy Institute, London, UK, UK.

[49] J. Black, 2013, *Cost and performance baseline for fossil energy plants volume 1: Bituminous coal and natural gas to electricity*, National Energy Technology Laboratory, Pittsburgh, PA, USA.

[50] B. Metz, O. Davidson, H. de Coninck, M. Loos, and L. Meyer, 2005, *IPCC special report on carbon dioxide capture and storage*, Cambridge University Press, Cambridge, United Kingdom and New York, NY, USA.

[51] T. Sanpasertparnich, R. Idem, I. Bolea, D. de Montigny, and P. Tontiwachwuthikul, 2010, "Integration of post-combustion capture and storage into a pulverized coal-fired power plant," *Int. J. Greenh. Gas Control*, 4, 3, 499–510.

[52] I. Pfaff, J. Oexmann, and A. Kather, 2010, "Optimised integration of post-combustion CO_2 capture process in greenfield power plants," *Energy*, 35, 10, 4030–4041.

[53] S. Posch and M. Haider, 2012, "Optimization of CO_2 compression and purification units (CO2CPU) for CCS power plants," *Fuel*, 101, 254–263.

[54] R. Peters, E. Riensche, and P. Cremer, 2000, "Pre-reforming of natural gas in solid oxide fuel-cell systems," *J. Power Sources*, 86, 1, 432–441.

[55] EG&G Technical Services, 2004, "Fuel Cell Handbook," *Fuel Cell*, 7 Edition, National Energy Technology Laboratory, Morgantown, WV, USA.

[56] J. C. Abanades, G. Grasa, M. Alonso, N. Rodriguez, E. J. Anthony, and L. M. Romeo, 2007, "Cost structure of a postcombustion CO_2 capture system using CaO," *Environ. Sci. Technol.*, 41, 15, 5523–5527.

[57] M. Zhao, A. I. Minett, and A. T. Harris, 2013, "A review of techno-economic models for the retrofitting of conventional pulverised-coal power plants for post-combustion capture (PCC) of CO_2," *Energy Environ. Sci.*, 6, 1, 25–40.

[58] Y. Yang, R. Zhai, L. Duan, M. Kavosh, K. Patchigolla, and J. Oakey, 2010, "Integration and evaluation of a power plant with a CaO-based CO_2 capture system," *Int. J. Greenh. Gas Control*, 4, 4, 603–612.

[59] A. Shirazi, M. Aminyavari, B. Najafi, F. Rinaldi, and M. Razaghi, 2012, "Thermal-economic-environmental analysis and multi-objective optimization of an internal-reforming solid oxide fuel cell-gas turbine hybrid system," *Int. J. Hydrogen Energy*, 37, 24, 19111–19124.

[60] Y. D. Lee, K. Y. Ahn, T. Morosuk, and G. Tsatsaronis, 2014, "Exergetic and exergoeconomic evaluation of a solid-oxide fuel-cell-based combined heat and power generation system," *Energy Convers. Manag.*, 85, 154–164.

[61] M. Aminyavari, A. H. Mamaghani, A. Shirazi, B. Najafi, and F. Rinaldi, 2016, "Exergetic, economic, and environmental evaluations and multi-objective optimization of an internal-reforming SOFC-gas turbine cycle coupled with a Rankine cycle," *Appl. Therm. Eng.*, 108, 833–846.

[62] M. H. Khoshgoftar Manesh, H. Ghalami, M. Amidpour, and M. H. Hamedi, 2013, "Optimal coupling of site utility steam network with MED-RO desalination through total site analysis and exergoeconomic optimization," *Desalination*, 316, 42–52.

[63] H. Sayyaadi and R. Mehrabipour, 2012, "Efficiency enhancement of a gas turbine cycle using an optimized tubular recuperative heat exchanger," *Energy*, 38, 1, 362–375.

[64] K. Atsonios, A. Koumanakos, K. D. Panopoulos, A. Doukelis, and E. Kakaras, 2013, "Techno-economic comparison of CO_2 capture technologies employed with natural gas derived GTCC," in *Proceedings of the ASME Turbo Expo*, 2.

[65] T. Kreutz, R. Williams, S. Consonni, and P. Chiesa, 2005, "Co-production of hydrogen, electricity and CO_2 from coal with commercially ready technology. Part B: Economic analysis," *Int. J. Hydrogen Energy*, 30, 7, 769–784.

[66] D. R. Woods, *Rules of thumb in engineering practice*. Weinheim, Germany: Wiley-VCH Verlag GmbH & Co. KGaA, 2007.

[67] R. H. Perry, D. W. Green, and J. O. Maloney, 2007, *Perry's chemical engineers' handbook*, McGraw-Hill, New York, NY, USA.

[68] A. Martínez, Y. Lara, P. Lisbona, and L. M. Romeo, 2014, "Operation of a mixing seal valve in calcium looping for CO_2 capture," *Energy and Fuels*, 28, 3, 2059–2068.

[69] P. Lisbona, A. Martínez, Y. Lara, and L. M. Romeo, 2010, "Integration of carbonate CO_2 capture cycle and coal-fired power plants. A comparative study for different sorbents," *Energy and Fuels*, 24, 1, 728–736.

[70] M. Krähenbühl, B. Etter, and K. M. Udert, 2016, "Pretreated magnesite as a source of low-cost magnesium for producing struvite from urine in Nepal," *Sci. Total Environ.*, 542, 1155–1161.

[71] M. C. Romano, I. Martínez, R. Murillo, B. Arstad, R. Blom, D. C. Ozcan, H. Ahn, and S. Brandani, 2013, "Process simulation of Ca-looping processes: Review and guidelines," *Energy Procedia*, 37, 142–150.

[72] D. P. Hanak, E. J. Anthony, and V. Manovic, 2015, "A review of developments in pilot plant testing and modelling of calcium looping process for CO_2 capture from power generation systems," *Energy Environ. Sci.*, 8, 2199–2249.

[73] P. Renforth, B. G. Jenkins, and T. Kruger, 2013, "Engineering challenges of ocean liming," *Energy*, 60, 442–452.

[74] P. Renforth and T. Kruger, 2013, "Coupling mineral carbonation and ocean liming," in *Energy and Fuels*, 27, 8, 4199–4207.

[75] P. Renforth, 2012, "The potential of enhanced weathering in the UK," *Int. J. Greenh. Gas Control*, 10, 229–243.

[76] H. S. Kheshgi, 1995, "Sequestering atmospheric carbon dioxide by increasing ocean alkalinity," *Energy*, 20, 9, 915–922.

[77] E. S. Rubin, C. Chen, and A. B. Rao, 2007, "Cost and performance of fossil fuel power plants with CO_2 capture and storage," *Energy Policy*, 35, 9, 4444–4454.

[78] EIA, 2016, *Levelized Cost and Levelized Avoided Cost of New Generation Resources in the Annual Energy Outlook 2016*, Washington, DC, USA.

[79] D. Berstad, R. Anantharaman, and K. Jordal, 2012, "Post-combustion CO_2 capture from a natural gas combined cycle by $CaO/CaCO_3$ looping," *Int. J. Greenh. Gas Control*, 11, 25–33.

[80] D. P. Hanak, A. J. Kolios, and V. Manovic, 2016, "Comparison of probabilistic performance of calcium looping and chemical solvent scrubbing retrofits for CO_2 capture from coal-fired power plant," *Appl. Energy*, 172, 323–336.

[81] D. P. Hanak, A. J. Kolios, C. Biliyok, and V. Manovic, 2015, "Probabilistic performance assessment of a coal-fired power plant," *Appl. Energy*, 139, 350–364.

[82] F. C. Veyo SE, 1998, "Demonstrations based on Westinghouse's prototype commercial," in *Proceedings of the Third European Solid Oxide Fuel Cell Forum*, 79–86.

[83] V. SE, 1996, "The Westinghouse solid oxide fuel cell program—a status report," in *Proceedings of the 31st Intersociety Energy Conversion Engineering Conference*, 1138–1143.

[84] L. W. Veyo S, 1999, "Solid oxide fuel cell power system cycles," in *International Gas Turbine and Aeroengine Congress and Exhibition*.

[85] W. Doherty, A. Reynolds, and D. Kennedy, 2010, "Computer simulation of a biomass gasification-solid oxide fuel cell power system using Aspen Plus," *Energy*, 35, 12, 4545–4555.

NOMENCLATURE

AC_k	Cross-section area of heat exchanger *k*	m^2
C_j	Capital cost of equipment *j*	£
CF	Capacity factor	-
e	Number of electrons produced per mole of H_2	-
e_{CO_2}	Specific negative CO_2 emission	$gCO_2/kW_{el}h$
F	Faraday constant	C/kmol
FCF	Fixed charge factor	-
FOM	Fixed operating and maintenance cost	£
I_C	Current density	mA/cm^2
I_{SOFC}	Solid-oxide fuel cell current	A
$LCOA$	Levelised cost of CO_2 capture from air	$£/tCO_2$
$LCOE$	Levelised cost of electricity	$£/MW_{el}h$
LHV	Lower heating value of fuel	kJ/kg
$\dot{m}_{calc}$	Calcined material production rate	kg/s
$\dot{m}_{CO_2}$	Rate of CO_2 removal from air	kg/s
$\dot{m}_{fuel}$	Fuel consumption rate	kg/s
$\dot{m}_{O_2}$	O_2 production rate in the air separation unit	kg/s
$\dot{n}_{H_2,eq}$	Equivalent H_2 molar flow rate	kmol/s
$\dot{n}_{i,in}$	Inlet molar flow rate of component *i* in the fresh fuel	kmol/s
$\dot{n}_{O_2,eq}$	Amount of O_2 consumed in the anode	kmol/s
P_{fuel}	Fuel inlet pressure	bar
P_i	Partial pressure of component *i* in the gas mixture	bar
$P_{i,ref}$	Reference partial pressure of component *i* in the gas mixture	bar
P_{ref}	Reference solid-oxide fuel cell operating pressure	bar
P_{SOFC}	Solid-oxide fuel cell operating pressure	bar
S/C	Steam-to-carbon ratio	-
SCF	Specific fuel cost	$£/MW_{el}h$
T_{ref}	Reference solid-oxide fuel cell operating temperature	°C
T_{SOFC}	Solid-oxide fuel cell operating temperature	°C
TCR	Total capital requirement	£
$\dot{Q}_k$	Heat transferred in heat exchanger *k*	kW_{th}
U_a	Air utilisation factor	-

U_f	Fuel utilisation factor	-
V_{ref}	Reference voltage	V
V_{SOFC}	Actual voltage of solid-oxide fuel cell	V
VOM	Variable operating and maintenance cost	£/$MW_{el}h$
$\dot{W}_{j,BRK}$	Break power output/requirement of equipment *j*	kW_{el}
$\dot{W}_{net}$	Net power output of the entire system	kW_{el}
$\dot{W}_{SOFC,AC}$	Solid-oxide fuel cell AC power output	kW_{el}
$\dot{W}_{SOFC,DC}$	Solid-oxide fuel cell DC power output	kW_{el}
$\Delta T_{LMTD,k}$	Log mean temperature difference in heat exchanger *k*	K
ΔV_{anode}	Reference voltage correction due to variation in the fuel composition	V
$\Delta V_{cathode}$	Reference voltage correction due to variation in the oxidant composition	V
ΔV_p	Reference voltage correction due to variation in the actual pressure	V
ΔV_T	Reference voltage correction due to variation in the actual temperature and current density	V
η_{BFP}	Isentropic efficiency of boiler feedwater pump	-
$\eta_{DC/AC}$	DC-to-AC inverter efficiency	-
η_{th}	Net thermal efficiency	-

ABBREVIATIONS

ASU	Air separation unit
CCU	CO_2 compression unit
DAC	Direct air capture
LCOA	Levelised cost of CO_2 capture from air
LCOE	Levelised cost of electricity
PR-BM	Peng-Robinson-Boston-Mathias
SOFC	Solid-oxide fuel cell